THE JOURNAL OF PHYSICAL CHEMISTRY Letters

Letter

pubs.acs.org/JPCL

Persistent Electronic Coherence Despite Rapid Loss of Electron–Nuclear Correlation

Alexey V. Akimov[†,‡] and Oleg V. Prezhdo*[,†]

[†]Department of Chemistry, University of Rochester, Rochester, New York 14627, United States

[‡]Department of Chemistry, Brookhaven National Laboratory, Upton, New York 11973, United States

ABSTRACT: Long-lived coherences of excited states are notable for their positive effect on energy conversion mechanisms and efficiencies in photosynthetic complexes. Rational engineering of such persistent coherences could open a new way to increase energy conversion rates in man-made photovoltaic and photocatalytic materials. Therefore, a comprehensive understanding of the fundamental principles behind the long-lived coherences is necessary. In this work we show that the main factor determining the decoherence rates is the magnitude of the nuclear-induced fluctuation of the energy gap between the electronic states of interest, rather than the electron–nuclear correlation on its own. Utilizing combined atomistic and electronic structure calculations, we demonstrate an inverse relationship between decoherence times and magnitude of the energy gap fluctuation. We also show that the energy gap fluctuation can often correlate with the gap itself. For sufficiently small energy gaps, the coherence time can be nearly an order of magnitude larger than the electron–nuclear correlation time.

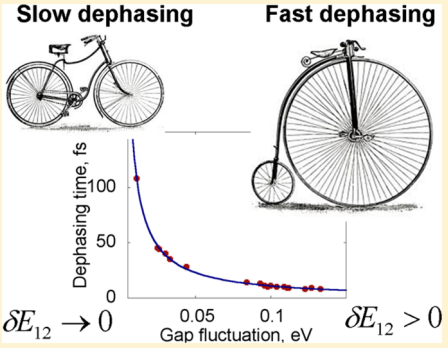

SECTION: Molecular Structure, Quantum Chemistry, and General Theory

Long-lived coherences of electronic states have been observed in many biological and molecular systems, in particular light-harvesting complexes.[1−4] As a consequence of such persistent coherences, wave-like energy transfer between system components facilitates robust mechanisms and higher efficiencies of solar energy harvesting and conversion into chemical energy.[1,5−7] The enhancement may stem from reversible energy storage in vibrational modes of the molecular environment, e.g., a protein, followed by energy extraction when needed.[5] A long-lived coherence could help to minimize energy losses and find a faster and energetically more favorable pathway for the energy transfer from the chromophore to the reaction center in photosynthetic systems.[8−13]

Inspired by nature's design, a number of artificial analogues of the biological light-harvesting complexes have been proposed and studied with the goal of creating materials for photovoltaic and photocatalytic applications. Despite the numerous experimental studies[1,14−16] and theoretical models,[15,17−23] there is still no consensus on the physical reason and microscopic origin of the long-lived coherences.

Often the persistent coherence in biological systems is attributed to a correlated nuclear motion of adjacent chromophores in a light-harvesting complex.[14,18] Correlated nuclear motions imply some degree of correlation of the electronic energy levels. Since evolution of the latter defines the rates of electronic dephasing, one may seek the origin of the long coherence times in the correlated evolution of the energy levels of the excited states.[20] For instance, long pure-dephasing times and narrow luminescence line-widths in carbon nanotubes at low temperatures can be attributed to such a mechanism.[24,25] The phonon modes of carbon nanotubes show little anharmonicity, especially near the energy minimum accessible at a low temperature. As a result, the electron–nuclear correlations persist for hundreds of femtoseconds, resulting in picosecond-long electronic coherences. However, it is important to recognize that, although electron–nuclear correlations and electronic coherences are closely related phenomena, other factors may play key roles.

In this Letter we show by computer simulation, applied to describe recently reported experimental data,[26] that a long-lived electronic coherence can exist even when the electron–nuclear correlations are short-lived. In this case, the main factor leading to development of a persistent electronic coherence is not the correlated evolution of energy levels, but rather it is a small magnitude of the fluctuation of the energy gap.

Typically, no differentiation of the contributions of the energy gap fluctuation and the electron–nuclear correlation to the coherence lifetime is made. Some authors associate extra-long coherence with extended electron–nuclear correlations,[14,18] including geometrical properties of molecular systems.[26] Others attribute it to a small magnitude of the energy gap,[19] which is not necessarily directly related to the gap fluctuation. One of the goals of the present work is to present a clear differentiation of the two factors, making it explicit how the electron–nuclear correlation and the energy gap fluctuation enter the decoherence function. In particular, we show with the

Received: September 20, 2013
Accepted: November 1, 2013
Published: November 1, 2013

   dx.doi.org/10.1021/jz402035z | J. Phys. Chem. Lett. 2013, 4, 3857−3864

concrete experimental system that a small energy gap fluctuation can lead to long coherences, even if the electron−nuclear correlation is quickly destroyed. This finding is rather counterintuitive and is extremely important. It should be kept in mind by experimentalists who design new systems exhibiting long coherence times.

The evolution of the energy levels shown in Figure 1 can be fully correlated: When the nuclear geometry evolves along a reaction coordinate, the energy change for one of the surfaces, e.g., ΔE_2, is related to the magnitude of the energy change for the other surface, ΔE_1. Despite the fact that the energy levels change in a correlated fashion, the energy gap $E_{12} = E_2 - E_1$ may experience different variations δE_{12} during the nuclear evolution, large (Figure 1a) or small (Figure 1b). Further, one can envision small, randomly fluctuating bumps in the potential energy surfaces along the reaction coordinate, for instance, arising due to coupling of the reaction coordinate to other vibrational modes. Then, the correlation in the fluctuations of the electronic energies will be rapidly lost, while the magnitude of the variation of the energy gap δE_{12} will remain approximately unchanged.

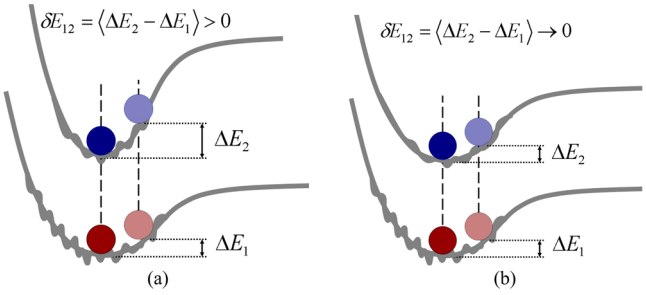

Figure 1. Mechanism of dephasing of a superposition of two electronic states due to coupling to nuclear motions. Wavepacket motion on two surfaces induces different changes in the potential energy. This leads to different magnitudes of the electronic energy gap fluctuation, δE_{12}. Faster dephasing corresponds to a larger energy gap fluctuation (a), while slower dephasing occurs when the gap fluctuation is smaller (b).

The correlation between the electronic energy levels i, j and the nuclear modes coupled to the electronic subsystem is quantified by the autocorrelation function (ACF) within the linear response theory. The unnonrmalized ACF (u-ACF), C_{ij}, is defined as

$$C_{ij}(t) = \langle \delta E_{ij}(t) \delta E_{ij}(0) \rangle \tag{1}$$

Here, $\delta E_{ij}(t) = E_{ij}(t) - \langle E_{ij} \rangle$ is the fluctuation of the energy gap $E_{ij}(t)$ between states i and j from its average value $\langle E_{ij} \rangle$. The angular brackets denote statistical mechanical averaging, in the present case performed over a canonical ensemble. Quantum-mechanical correlation functions are generally complex. Classical molecular dynamics allows one to sample efficiently the real part of the ACF, entering the semiclassical expression for the decoherence/pure-dephasing function of the optical response theory.[27]

The normalized ACF (n-ACF), $\tilde{C}_{ij}$, is related to the u-ACF by the mean-square fluctuation (variance) of the energy gap between the two states involved in the coherent superposition, $\langle \delta E_{ij}^2 \rangle$:

$$\tilde{C}_{ij}(t) = \frac{C_{ij}}{\langle \delta E_{ij}^2 \rangle} = \frac{\langle \delta E_{ij}(t) \delta E_{ij}(0) \rangle}{\langle \delta E_{ij}^2 \rangle} \tag{2}$$

The Fourier transform (FT)

$$I_{ij}(\omega) = \frac{1}{2\pi} \left| \int_{-\infty}^{+\infty} \mathrm{d}t e^{-i\omega t} \tilde{C}_{ij}(\omega) \right|^2 \tag{3}$$

of the n-ACF gives the spectral density, also known as the influence spectrum. The influence spectrum identifies the vibrational modes that are strongly coupled to the electronic subsystem. The pure-dephasing function of the optical response theory is often used to quantify the coherence time.[27,28] The inverse of the pure-dephasing time gives the experimentally measurable homogeneous line-width of an optical transition. The pure-dephasing function is defined in the second-order cumulant approximation[27] as

$$D_{ij}(t) = \exp\left[-\frac{1}{\hbar^2} \int_0^t \mathrm{d}t' \int_0^{t'} \mathrm{d}t'' C_{ij}(t'') \right] \tag{4}$$

where the u-ACF is utilized, eq 1.

To illustrate that long-lived coherences are possible even when the electron−nuclear correlation decays rapidly, we focus on a series of organic heterodimers, recently studied experimentally by the Engel group.[26] The 2D spectroscopy measurements indicate that the coherences between the first

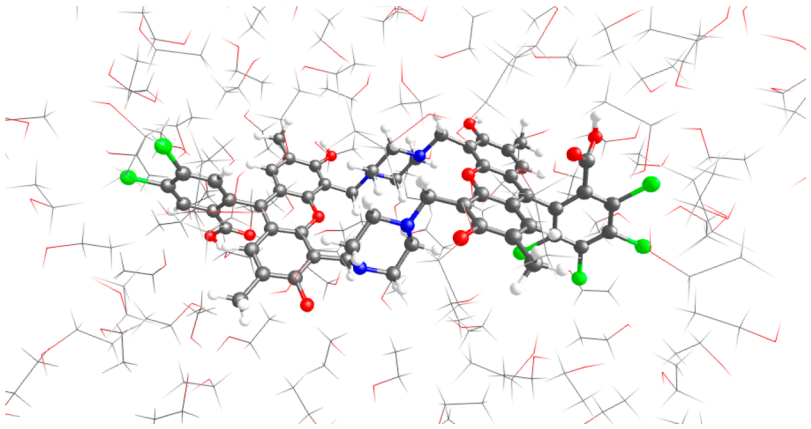

Figure 2. The AB heterodimer in the EtOH solvent box. The color codes of the atoms in the heterodimer molecule are: gray − carbon, white − hydrogen, blue − nitrogen, red − oxygen, and green − chlorine. Solvent EtOH molecules are shown in the wireframe representation; the solute AB dimer is shown in the ball-and-stick representation.

dx.doi.org/10.1021/jz402035z | J. Phys. Chem. Lett. 2013, 4, 3857−3864

two excited states in these systems are preserved for nearly an order of magnitude longer than coherences between each individual excited state and the ground state. Since the two excited states are localized on different fragments of the dimer, the experiment shows that the coherences involved in energy transfer between the fragments live much longer than the coherences created by photoexcitation. Engel and co-workers[26] considers three heterodimers denoted by AB, AC, and BC, dissolved in ethanol (EtOH). The monomeric units A, B, and C are the 5,6-dichloro-2′,7′-dimethylfluorescein, 4,5,6,7-tetrachloro-2′,7′-dimethylfluorescein, and 4,5,6,7-tetrachloro-2′,7′-dichlorofluorescein, respectively. In our computational studies, we consider exactly the same systems, as those used in the experiment. In addition, we consider the dimers in vacuum and in $CHCl_3$ that represents a polar, non-hydrogen bonding solvent. The molecular structure of the AB heterodimer solvated by ethanol is presented in Figure 2.

To model the electron−nuclear dynamics in such complex systems, we combine classical molecular dynamics (MD) and semiempirical extended Hückel theory (EHT). We utilize the CHARMM general force field[29] to describe bonded and nonbonded nonelectrostatic molecular interactions. Electrostatic interactions are taken into account using Gasteiger[30] charges on all atoms and a particle-mesh Ewald summation with the 10^{-6} kcal/mol accuracy. A simulation cell of 35 × 20 × 20 Angstrom is used, which allows us to consider explicitly about 100 EtOH solvent molecules, totaling in about 1200 atoms. Periodic boundary conditions are used to minimize spurious finite-size effects.

100 ps long molecular dynamics trajectories are obtained using the velocity Verlet algorithm[31] with the integration time step of 1 fs. To maintain the constant temperature of 300 K we utilize the Langevin dynamics[32] with the collision frequency of 10 ps^{-1}. The first 50 ps of the computed trajectories are considered thermalization period and are disregarded. Because the coordinates are stored every 1 fs, resulting in excessively large data files, the reported data are obtained by computing electronic structure and averaging over 10 ps. All molecular dynamics simulations and trajectory manipulations are performed using the NAMD package[33] and the VEGA ZZ interface.[34]

To obtain the electronic energy levels, we perform EHT calculations[35] using the YAeHMOP package.[36] The relevant molecular orbitals (MOs) are visualized using the Argus Lab software.[37] In order to further analyze the nature of the lowest energy excitations in the systems under investigation, we carry out configuration interaction (CI) calculations with the semiempirical ZINDO[38] Hamiltonian. The EHT methodology often provides good results for organic molecules,[35,39] inorganic species,[40−42] carbon nanotubes,[43] solid-state materials,[44] and interfacial systems.[45−48] For example, it has been used extensively by the Batista group to study electron transfer in dye-sensitized solar cells.[49−52] To achieve computational savings, the EHT calculations are performed on finite size clusters, taken from the periodic simulation cell of classical MD. Such clusters include both the dimer molecule and a solvent layer that is sufficiently large to encompass the solute completely. This should be a valid approximation, because the majority of the solvent effects is well represented by the first and second solvation shells.[53−55]

The hybrid molecular-mechanics/semiempirical methodology described above enables us to obtain converged statistical averages in complex molecular systems at a very low computational cost. The MD computations for each system take approximately 1 h of CPU time on a standard PC. The EHT step performed in a high-throughput manner takes less than a day on a Linux cluster. In comparison, ab initio DFT band structure calculations with a limited number of solvent molecules would take months, yet provide a comparable accuracy.[56−58] Therefore, our methodology constitutes a valuable tool for express evaluation of coherences in large condensed matter and molecular systems.

To understand the nature of the lowest excited states in the molecular dimers, we analyze the frontier one-electron wave functions, computed at the EHT level of theory, and compare the results to the CI calculations with the ZINDO[38] Hamiltonian. The representative snapshots of MOs of the AB dimer, computed in vacuum, are shown in Figure 3. The

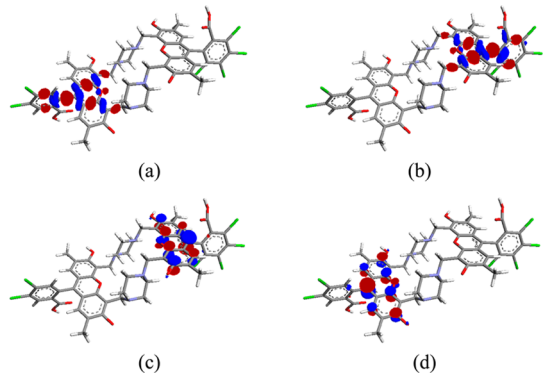

Figure 3. Frontier molecular orbitals of the AB dimer in vacuum obtained with the EHT method: (a) HOMO-1; (b) HOMO; (c) LUMO; (d) LUMO+1. The orbital isosurface value is 0.05 au.

HOMO-1 and LUMO+1 are localized on one of the monomers, while the HOMO and LUMO localize on the other monomer. Therefore, due to strong orbital overlap, the HOMO → LUMO and HOMO-1 → LUMO+1 transitions are the most optically active, and represent the dominant contributions to the excited states studied experimentally by the Engel group. These states will be referred to as states 1 and 2, while the ground-state configurations will be labeled as state 0. The orbital energy differences representing the 0→1 and 0→2 transitions underestimate the corresponding experimental values, while the 1→2 gaps are slightly larger than the experimental data. For consistency with experiment, and because of the increased importance of the accuracy in the transition energy for small gaps, we scaled the average computed 0→1 and 1→2 energies to the experimental values, by multiplying the gaps by a constant.

We want to emphasize that the scaling of the energy levels does not affect the qualitative conclusions made in this work. The scaling is only necessary in order to ensure quantitative comparison with the experiment: for the calculated dephasing times to be correctly compared with those measured in the experiment, the energy gaps should also be comparable. One cannot expect the semiempirical EHT method to achieve accuracy on the order of 0.01 eV. Such a great accuracy can hardly be achieved even with sophisticated ab initio methods. Therefore, the only possibility to make a quantitative comparison with experiment is to perform the empirical scaling. The 0→1 gaps are 2.37, 2.30, and 2.28 eV for the AB, AC, and BC dimers, respectively. The 1→2 gaps are given in Table 1.

dx.doi.org/10.1021/jz402035z | J. Phys. Chem. Lett. 2013, 4, 3857−3864

Table 1. Comparison of the Dephasing Times, Energy Gaps and Gap Fluctuations for the 1→2 Transition in the Three Dimers[a]

	AB	AC	BC
experimental dephasing time, fs	90	60	60
computed dephasing time, τ_{ij}, fs	45	28	108
electronic energy gap, $\langle E_{ij} \rangle$, eV	0.06	0.09	0.02
gap fluctuation, $\langle \delta E_{ij}^2 \rangle^{1/2}$, eV	0.025	0.044	0.011

[a]Since the uncertainty in the experimental dephasing times is large, possibly as large as the dephasing time itself,[26] the calculated values are in agreement with the experiment.

The EHT calculations are supported by our ZINDO CI calculations. The CI expansions show that the HOMO → LUMO and HOMO-1 → LUMO+1 transitions indeed give the largest contributions to the optically active excitations. ZINDO CI produces better excitation energies; however, it is computationally more expensive than EHT, especially with explicit solvent. We would like to emphasize that the key message of the manuscript is independent of the details of the electronic structure computations.

The computed n-ACFs for the 0→1, 0→2, and 1→2 gaps of the AB dimer are presented in Figure 4a. They show that the electron−nuclear correlation decays on a 20 fs time-scale, and that the time-scale is nearly system independent. At the same time, the decoherence functions, presented in Figure 4b, show that coherence between states 1 and 2 is preserved for much longer time than coherence between states 0−1 and 0−2. Namely, while each of the excited states dephases with respect to the ground state on a 10 fs time-scale, the coherence between the pair of excited states is preserved for as long as 50 fs. The coincidence between the correlation and coherence times for the 0→1 and 0→2 excitations is fortuitous. Note that the computed coherence times for the 0→1 and 0→2 transitions are in excellent agreement with the experimental values of less than 15 fs.[26] Figure 4 illustrates that coherences may be preserved for times longer than the correlation times, especially when the energy gaps are small.

The spectral density, also known as the influence spectrum, is shown in the inset of Figure 4b. It identifies the vibration modes that are responsible for dephasing of a given pair of states. In all cases, low-frequency modes, especially those below 500 cm^{-1}, dominate the dephasing process. These types of vibrations correspond to collective motions of the molecule and its groups within a solvent network, as well as the out-of-plane vibrations of planar molecular fragments. The intensity of the peaks in the influence spectrum characterizes the strength of the electron−nuclear coupling. The coupling is weaker for the 1→2 excitation than for the 0→1 and 0→2 excitations. High-frequency modes at 1600−1900 cm^{-1} exhibit minor intensity and can be attributed to intramolecular C−C and C−O bond stretching.

To study the effect of the molecular structure on the decoherence time, we consider all three heterodimers used in the experimental studies by the Engel group.[26] The results of our calculations for the 1→2 excitation are presented in Figure 5. Again, the n-ACF decays very fast, on a 20 fs time-scale, and is hardly affected by the molecular structure, Figure 5a. In contrast, the dephasing function is very sensitive to the relatively small structural changes of the molecules, Figure 5b. The dephasing times vary significantly among the dimers, and the difference between the time-scales for the electron−nuclear correlation and the vibrationally induced decoherence in the electronic subsystem is nearly an order of magnitude for the BC system. Note that the BC dimer has the smallest gap between states 1 and 2 (Table 1).

It is important to emphasize that the strong dependence of the coherence times on minor structural changes implies that the electronic-nuclear correlation is not a major factor leading to the long times for electronic coherences in the presently studied systems. Instead, purely electronic effects appear to be more important. Small structural changes can notably influence the electronic structure, especially the magnitudes of the energy gap between the two states and the gap fluctuation.

The computed and experimentally measured decoherence times for the 1→2 transition exhibiting long-lived coherence are summarized in Table 1. The decoherence times, τ_{ij}, were obtained by fitting the dephasing functions, eq 4, with a Gaussian.

$$D_{ij}(t) = \exp\left(-\left(\frac{t}{\tau_{ij}}\right)^2\right) \tag{5}$$

Our results are in agreement with the measured values. The experimental data have large uncertainties; the error in the dephasing time is greater than the dephasing time itself.[26] The computed dephasing times between the ground and each excited state are 10 fs (Figure 4b) and are in excellent agreement with experimental values of less than 15 fs.[26]

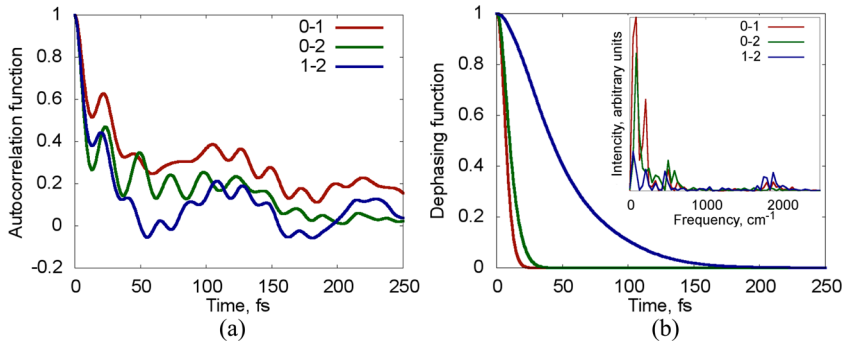

Figure 4. (a) Normalized autocorrelation function, eq 2, and (b) dephasing function, eq 4, for the three electronic transitions in the AB molecular heterodimer in the EtOH solvent. 0, 1, and 2 refer to the ground, first, and second excited states. The spectral density, eq 3, is shown as an inset in panel (b).

dx.doi.org/10.1021/jz402035z | J. Phys. Chem. Lett. 2013, 4, 3857−3864

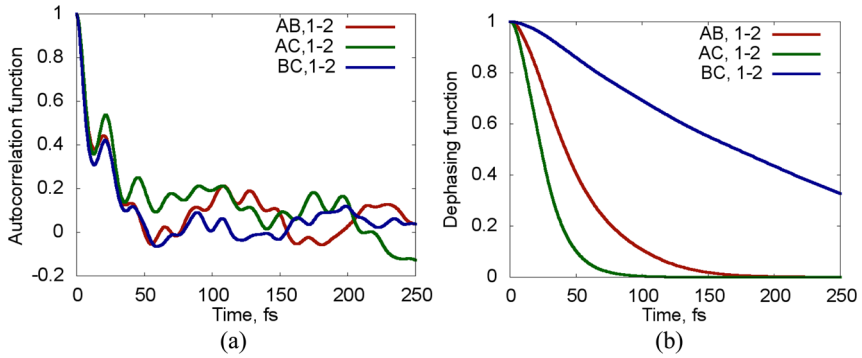

Figure 5. (a) Normalized autocorrelation function, eq 2, and (b) dephasing function, eq 4, for the transitions between the first and second excited states in the AB, AC, and BC dimers in the EtOH solvent. Panel (a) describes the correlation of the vibrationally induced fluctuations of donor and acceptor electronic levels. Panel (b) describes time-evolution of the coherences between the given pairs of states. The electronic coherence between the two excited states varies 5-fold among the three dimers, while the electron−nuclear correlation is very similar in all dimers. Remarkably, the coherence time can be an order of magnitude larger than the correlation time.

One observes an inverse relationship between the computed dephasing times and the standard deviation of the energy gap, $\langle \delta E_{ij}^2 \rangle^{1/2}$, which we call the energy gap fluctuation: the smaller the fluctuation, the larger the dephasing time. This relation is consistent with other theoretical works that list the energy gap fluctuation among the factors leading to the long-lived electronic coherences.[20,23] The same relation is consistent with the Förster resonant energy transfer framework.[59] One also observes a linear correlation between the magnitudes of the energy gap and its fluctuation. This relation is consistent with the result of the spin-boson model of Pachon and Brumer.[19] The linear correlation between the gap and its fluctuation is approximate; however, it is quite useful, since the average gap value is readily available experimentally, while estimating gap fluctuation requires elimination of inhomogeneous spectral broadening. The inverse correlation between the dephasing time and the gap fluctuation is very accurate for the present systems.

To test the universality of the inverse relation between the dephasing times and the energy gap fluctuation, $\langle \delta E_{ij}^2 \rangle^{1/2}$, we plotted the computed dephasing times versus the energy gap fluctuation in Figure 6. The data include all pairs of states (0→1, 0→2, and 1→2) for all heterodimers (AB, AC, and BC) in EtOH and for the AB dimer in $CHCl_3$ and vacuum. The $f(x) = A/x + B$ function gives a perfect fit, supporting the conclusion that the persistent coherence between the excited states arises due to the small energy gap, rather than a long electron−nuclear correlation time.

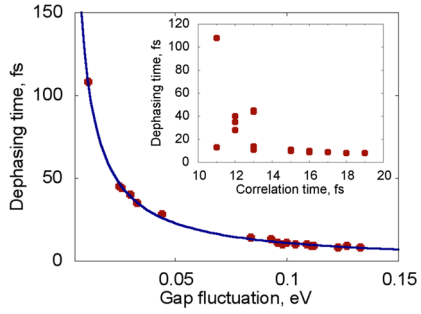

Figure 6. Dependence of the calculated dephasing times, τ_{ij}, on the fluctuation of the electronic energy gap, $\langle \delta E_{ij}^2 \rangle^{1/2}$, for the three molecular dimers in different solvents. The dots represent the calculated values, and the solid line represents the fitting function, $f(x) = A/x + B$. The fitting constants are $A = 1.20 \pm 0.01$ eV·fs and $B = -1.10 \pm 0.32$ fs. The inset shows dephasing time versus the time-scale of the initial n-ACF decay, accounting for 50% of the overall decay amplitude. Some points in the insert have close values along the y-axis, and coalesce.

The inverse relation between the decoherence time and the energy gap fluctuation obtained empirically from the atomistic simulations can be rationalized by analysis of the normalized and unnormalized ACFs, eqs 1, 2, and their relation to the energy gap fluctuation and the dephasing function, eq 4. The decoherence time is defined by the Gaussian fit of the decoherence function, eq 5. Taking the logarithm of both sides and using eqs 1, 2, and 4, one obtains

$$\left(\frac{t}{\tau_{ij}}\right)^2 = \frac{1}{\hbar^2}\int_0^t dt' \int_0^{t'} dt'' C_{ij}(t'') = \frac{\langle \delta E_{ij}^2 \rangle}{\hbar^2}\int_0^t dt' \int_0^{t'} dt'' \tilde{C}_{ij}(t'') \quad (6)$$

The double integral in the right-hand side of eq 6 is related to the decoherence function with the average energy fluctuation equal to unity (e.g., 1 eV, if the energy units are set to eV),

$$\tilde{D}_{ij}(t) = \exp\left[-\frac{1}{\hbar^2}\int_0^t dt' \int_0^{t'} dt'' \tilde{C}_{ij}(t'')\right] = \exp\left(-\left(\frac{t}{\tilde{\tau}_{ij}}\right)^2\right) \quad (7)$$

$\tilde{D}_{ij}(t)$ shows Gaussian behavior, similarly to $D_{ij}(t)$, but with a different time-scale, $\tilde{\tau}_{ij}$. By comparing eqs 6 and 7, one can derive

$$\tau_{ij}^2 = \frac{\tilde{\tau}_{ij}^2}{\langle \delta E_{ij}^2 \rangle} \quad (8)$$

and, finally

$$\tau_{ij} = \frac{\tilde{\tau}_{ij}}{\langle \delta E_{ij}^2 \rangle^{1/2}} \quad (9)$$

The above derivations show that the decoherence function can exhibit slow decay if the fluctuation of the electronic energy gap, $\langle \delta E_{ij}^2 \rangle^{1/2}$, is small. The proportionality constant, $\tilde{\tau}_{ij}$,

dx.doi.org/10.1021/jz402035z | J. Phys. Chem. Lett. 2013, 4, 3857−3864

represents the decoherence time for a fixed energy gap fluctuation of 1.0 eV, and hence is independent of the gap fluctuation.

Moreover, one can show that the decoherence time, τ_{ij}, is approximately independent of the electron nuclear correlation time, $\tau_{\mathrm{corr},ij}$. The initial decay of the n-ACF is approximately Gaussian and accounts for 50% of the overall n-ACF decay, Figures 4 and 5. We define the nuclear correlation time by fitting the initial part of the n-ACF to a Gaussian

$$\tilde{C}_{ij}(t) \equiv \exp\left(-\left(\frac{t}{\tau_{\mathrm{corr},ij}}\right)^2\right) \tag{10}$$

Next, we consider the first two terms in the Taylor expansion of eq 10, which give rise to the short-term, parabolic part of the n-ACF decay. Using the expansion, we compute both sides of eq 7 at the correlation time, leading to

$$\begin{aligned} -\frac{1}{\hbar^2}\int_0^{\tau_{\mathrm{corr}}} \mathrm{d}t' \int_0^{t'} \mathrm{d}t'' \tilde{C}_{ij}(t'') &= -\frac{1}{\hbar^2}\left(\frac{\tau_{\mathrm{corr}}^2}{2} - \frac{\tau_{\mathrm{corr}}^2}{12}\right) \\ &= -\frac{\tau_{\mathrm{corr}}^2}{\tilde{\tau}_{ij}^2} \end{aligned} \tag{11}$$

and hence

$$\tilde{\tau}_{ij} = \hbar\sqrt{\frac{12}{5}} \approx 1.02\ \mathrm{eV{\cdot}fs} \tag{12}$$

Finally,

$$\tau_{ij} = \frac{1.02\ \mathrm{eV{\cdot}fs}}{\langle \delta E_{ij}^2 \rangle^{1/2}} \tag{13}$$

independent of the electron−nuclear correlation time, $\tau_{\mathrm{corr},ij}$.

The constant obtained in eq 12 agrees perfectly with the proportionality constant A (Figure 6), obtained from the direct calculations. Most importantly, eqs 12 and 13 emphasize the fact that the decoherence time is independent of the electron−nuclear correlation time.

To test the last conclusion, we present the plot of the decoherence time, τ_{ij}, versus the correlation time, τ_{corr}, on the inset in Figure 6. One observes no monotonic relationship between the two time-scales. Moreover, several decoherence times can correspond to the same electron−nuclear correlation time. Alternatively, different electron−nuclear correlation times lead to practically the same decoherence time. In a number of cases, the electron−nuclear correlation time is extremely small, while the decoherence time is significantly larger.

We want to emphasize that one cannot obtain a comprehensive insight into the mechanism of long-lived coherences by analyzing the spectral density only. This is because the spectral density is computed using the n-ACF, and therefore reflects only the electron−nuclear correlation time, τ_{corr}. The decoherence times are obtained using the u-ACF, which depends on the energy gap fluctuation. Even if the electron−nuclear correlation is quickly lost, there is a chance that long coherences can be observed.

The established inverse relationship between the energy gap fluctuation and coherence time is consistent with the exchange narrowing mechanism proposed by Knapp.[17] According to this mechanism, intersite coupling between chromophore units results in exciton delocalization. As a consequence, local inhomogeneities present at individual molecular sites are averaged out, leading to longer coherence times. The Knapp model can be rationalized from the point of view of the energy gap fluctuations: averaging of the local site inhomogeneities leads to smaller energy gap fluctuations, and hence to longer dephasing times.

The strong intersite coupling model presents one mechanism for long coherence. Other possibilities include weak electron-vibrational coupling and small gaps. If the gap fluctuation is large, then long-lived coherences do require long-lasting electron−nuclear correlations, as exemplified by the coherence between the ground and first excited states of carbon nanotubes at low temperatures.[24]

In this work, we argue that correlated electron−nuclear motions may not be necessary to achieve long coherence times. The exact mechanisms leading to small energy gap fluctuations may differ from system to system. For example, as shown by J. Cao et al.,[10] biological systems function under the optimal condition, where the strength of electron−nuclear coupling is comparable with excitonic coupling. In this regime, the true eigenstates are not excitonic states, but rather polaron states. Under these conditions, the line-shape function used in the present analysis may be modified, possibly affecting the inverse relationship between the energy gap fluctuation and the decoherence time.

To summarize, we have studied a series of solvated heterodimer molecules, representing biological light-harvesting and photosynthetic systems. By combining classical MD and EHT, we have been able to study systems with over 1000 atoms and to achieve canonical averaging over tens of picoseconds. The generated data have allowed us to perform express-evaluation of the electronic coherence and electron−nuclear correlation times in these systems. We show that the rapid decay of the electron−nuclear correlation is independent of the transition type and molecular structure. At the same time, the electronic coherence does depend strongly on both the type of transition and molecular structure. In particular, the dephasing times are inversely proportional to the magnitude of the fluctuation of the electronic energy gap and are independent of the electron−nuclear correlation time-scale. Since the average gap value is much easier to measure than the gap fluctuation, we have shown that the gap fluctuation may be approximately linear with the gap magnitude. The linear relationship is expected to work within a series of homological molecules, such as heterodimers, but may not always be transferred across different classes of systems. Finally, we have demonstrated that long-lived coherence can be achieved even if the electron−nuclear correlation is short. Our study reveals a fundamental mechanism behind the persistent coherences in light harvesting systems and provides a principle for rational design of long-lived electronic coherences in novel nanoscale materials.

AUTHOR INFORMATION

Notes

The authors declare no competing financial interest.

ACKNOWLEDGMENTS

A.V.A was funded by the Computational Materials and Chemical Sciences Network (CMCSN) project at Brookhaven National Laboratory under Contract DE-AC02-98CH10886 with the U.S. Department of Energy and supported by its

Division of Chemical Sciences, Geosciences & Biosciences, Office of Basic Energy Sciences. O.V.P. acknowledges financial support of the U.S. Department of Energy, Grant DE-SC0006527.

REFERENCES

(1) Engel, G. S.; Calhoun, T. R.; Read, E. L.; Ahn, T.-K.; Mančal, T.; Cheng, Y.-C.; Blankenship, R. E.; Fleming, G. R. Evidence for Wavelike Energy Transfer through Quantum Coherence in Photosynthetic Systems. *Nature* **2007**, *446*, 782−786.
(2) Westenhoff, S.; Paleček, D.; Edlund, P.; Smith, P.; Zigmantas, D. Coherent Picosecond Exciton Dynamics in a Photosynthetic Reaction Center. *J. Am. Chem. Soc.* **2012**, *134*, 16484−16487.
(3) Kreisbeck, C.; Kramer, T. Long-Lived Electronic Coherence in Dissipative Exciton Dynamics of Light-Harvesting Complexes. *J. Phys. Chem. Lett.* **2012**, *3*, 2828−2833.
(4) Fidler, A. F.; Singh, V. P.; Long, P. D.; Dahlberg, P. D.; Engel, G. S. Time Scales of Coherent Dynamics in the Light-Harvesting Complex 2 (LH2) of *Rhodobacter Sphaeroides*. *J. Phys. Chem. Lett.* **2013**, *4*, 1404−1409.
(5) Panitchayangkoon, G.; Voronine, D. V.; Abramavicius, D.; Caram, J. R.; Lewis, N. H.; Mukamel, S.; Engel, G. S. Direct Evidence of Quantum Transport in Photosynthetic Light-harvesting Complexes. *Proc. Natl. Acad. Sci. U. S. A.* **2011**, *108*, 20908−20912.
(6) Strümpfer, J.; Şener, M.; Schulten, K. How Quantum Coherence Assists Photosynthetic Light-Harvesting. *J. Phys. Chem. Lett.* **2012**, *3*, 536−542.
(7) Kassal, I.; Yuen-Zhou, J.; Rahimi-Keshari, S. Does Coherence Enhance Transport in Photosynthesis? *J. Phys. Chem. Lett.* **2013**, *4*, 362−367.
(8) Wu, J.; Liu, F.; Ma, J.; Silbey, R. J.; Cao, J. Efficient Energy Transfer in Light-Harvesting Systems: Quantum-Classical Comparison, Flux Network, and Robustness Analysis. *J. Chem. Phys.* **2012**, *137*, 174111.
(9) Moix, J. M.; Khasin, M.; Cao, J. Coherent Quantum Transport in Disordered Systems: I. The Influence of Dephasing on the Transport Properties and Absorption Spectra on One-Dimensional Systems. *New J. Phys.* **2013**, *15*, 085010.
(10) Wu, J.; Silbey, R. J.; Cao, J. Generic Mechanism of Optimal Energy Transfer Efficiency: A Scaling Theory of the Mean First-Passage Time in Exciton Systems. *Phys. Rev. Lett.* **2013**, *110*, 200402.
(11) Kolli, A.; O'Reilly, E. J.; Scholes, G. D.; Olaya-Castro, A. The Fundamental Role of Quantized Vibrations in Coherent Light Harvesting by Cryptophyte Algae. *J. Chem. Phys.* **2012**, *137*, 174109.
(12) Hossein-Nejad, H.; Olaya-Castro, A.; Scholes, G. D. Phonon-Mediated Path-Interference in Electronic Energy Transfer. *J. Chem. Phys.* **2012**, *136*, 024112.
(13) Fujita, T.; Brookes, J. C.; Saikin, S. K.; Aspuru-Guzik, A. Memory-Assisted Exciton Diffusion in the Chlorosome Light-Harvesting Antenna of Green Sulfur Bacteria. *J. Phys. Chem. Lett.* **2012**, *3*, 2357−2361.
(14) Lee, H.; Cheng, Y.-C.; Fleming, G. R. Coherence Dynamics in Photosynthesis: Protein Protection of Excitonic Coherence. *Science* **2007**, *316*, 1462−1465.
(15) Christensson, N.; Milota, F.; Hauer, J.; Sperling, J.; Bixner, O.; Nemeth, A.; Kauffmann, H. F. High Frequency Vibrational Modulations in Two-Dimensional Electronic Spectra and Their Resemblance to Electronic Coherence Signatures. *J. Phys. Chem. B* **2011**, *115*, 5383−5391.
(16) Tiwari, V.; Peters, W. K.; Jonas, D. M. From the Cover: Electronic Resonance with Anticorrelated Pigment Vibrations Drives Photosynthetic Energy Transfer Outside the Adiabatic Framework. *Proc. Natl. Acad. Sci. U. S. A.* **2012**, *110*, 1203−1208.
(17) Knapp, E. W. Lineshapes of Molecular Aggregates, Exchange Narrowing and Intersite Correlation. *Chem. Phys.* **1984**, *85*, 73−82.
(18) Souaille, M.; Marchi, M. Nuclear Dynamics and Electronic Transition in a Photosynthetic Reaction Center. *J. Am. Chem. Soc.* **1997**, *119*, 3948−3958.
(19) Pachón, L. A.; Brumer, P. Physical Basis for Long-Lived Electronic Coherence in Photosynthetic Light-Harvesting Systems. *J. Phys. Chem. Lett.* **2011**, *2*, 2728−2732.
(20) Christensson, N.; Kauffmann, H. F.; Pullerits, T.; Mančal, T. Origin of Long-Lived Coherences in Light-Harvesting Complexes. *J. Phys. Chem. B* **2012**, *116*, 7449−7454.
(21) Balevičius, V.; Gelzinis, A.; Abramavicius, D.; Mančal, T.; Valkunas, L. Excitation Dynamics and Relaxation in a Molecular Heterodimer. *Chem. Phys.* **2012**, *404*, 94−102.
(22) Kim, H. W.; Kelly, A.; Park, J. W.; Rhee, Y. M. All-Atom Semiclassical Dynamics Study of Quantum Coherence in Photosynthetic Fenna−Matthews−Olson Complex. *J. Am. Chem. Soc.* **2012**, *134*, 11640−11651.
(23) Shim, S.; Rebentrost, P.; Valleau, S.; Aspuru-Guzik, A. Atomistic Study of the Long-Lived Quantum Coherences in the Fenna−Matthews−Olson Complex. *Biophys. J.* **2012**, *102*, 649−660.
(24) Habenicht, B. F.; Kamisaka, H.; Yamashita, K.; Prezhdo, O. V. Ab Initio Study of Vibrational Dephasing of Electronic Excitations in Semiconducting Carbon Nanotubes. *Nano Lett.* **2007**, *7*, 3260−3265.
(25) Habenicht, B.; Prezhdo, O. Nonradiative Quenching of Fluorescence in a Semiconducting Carbon Nanotube: A Time-Domain Ab Initio Study. *Phys. Rev. Lett.* **2008**, *100*, 197402.
(26) Hayes, D.; Griffin, G. B.; Engel, G. S. Engineering Coherence Among Excited States in Synthetic Heterodimer Systems. *Science* **2013**, *340*, 1431−1434.
(27) Mukamel, S. *Principles of Nonlinear Optical Spectroscopy*; Oxford University Press: New York, 1995.
(28) Madrid, A. B.; Hyeon-Deuk, K.; Habenicht, B. F.; Prezhdo, O. V. Phonon-induced Dephasing of Excitons in Semiconductor Quantum Dots: Multiple Exciton Generation, Fission, and Luminescence. *ACS Nano* **2009**, *3*, 2487−2494.
(29) Vanommeslaeghe, K.; Hatcher, E.; Acharya, C.; Kundu, S.; Zhong, S.; Shim, J.; Darian, E.; Guvench, O.; Lopes, P.; Vorobyov, I.; et al. CHARMM General Force Field: A Force Field for Drug-like Molecules Compatible with the CHARMM All-atom Additive Biological Force Fields. *J. Comput. Chem.* **2010**, *31*, 671−690.
(30) Gasteiger, J.; Marsili, M. Iterative Partial Equalization of Orbital Electronegativity—A Rapid Access to Atomic Charges. *Tetrahedron* **1980**, *36*, 3219−3228.
(31) Verlet, L. Computer "Experiments" on Classical Fluids. I. Thermodynamical Properties of Lennard-Jones Molecules. *Phys. Rev.* **1967**, *159*, 98−103.
(32) Andersen, H. C. Molecular Dynamics Simulations at Constant Pressure and/or Temperature. *J. Chem. Phys.* **1980**, *72*, 2384−2393.
(33) Phillips, J. C.; Braun, R.; Wang, W.; Gumbart, J.; Tajkhorshid, E.; Villa, E.; Chipot, C.; Skeel, R. D.; Kale, L.; Schulten, K. Scalable Molecular Dynamics with NAMD. *J. Comput. Chem.* **2005**, *26*, 1781−1802.
(34) Pedretti, A.; Villa, L.; Vistoli, G. VEGA: A Versatile Program to Convert, Handle and Visualize Molecular Structure on Windows-Based PCs. *J. Mol. Graphics* **2002**, *21*, 47−49.
(35) Hoffmann, R. An Extended Hückel Theory. I. Hydrocarbons. *J. Chem. Phys.* **1963**, *39*, 1397.
(36) Landrum, G. A.; Glassey, W. V. Bind (ver 3.0). Bind is distributed as part of the YAeHMOP Extended Huckel Molecular Orbital Package and is freely available on the world-wide web at http://sourceforge.net/projects/yaehmop.
(37) Thompson, M. A. *ArgusLab 4.0*; Planaria Software LLC, Seattle, WA, 2008 (http://arguslab.com).
(38) Zerner, M. C.; Loew, G. H.; Kirchner, R. F.; Mueller-Westerhoff, U. T. An Intermediate Neglect of Differential Overlap Technique for Spectroscopy of Transition-Metal Complexes. Ferrocene. *J. Am. Chem. Soc.* **1980**, *102*, 589−599.
(39) Hoffmann, R. Extended Hückel Theory. II. σ Orbitals in the Azines. *J. Chem. Phys.* **1964**, *40*, 2745.
(40) Pyykkö, P.; Lohr, L. L., Jr. Relativistically Parameterized Extended Hueckel Calculations. 3. Structure and Bonding for Some Compounds of Uranium and Other Heavy Elements. *Inorg. Chem.* **1981**, *20*, 1950−1959.

(41) Pyykkö, P.; Laaksonen, L. Relativistically Parameterized Extended Huckel Calclulations. 8. Double-Zeta Parameters for the Actinoids Th, Pa, U, Np, Pu, and Am and Application on Uranyl. *J. Phys. Chem.* **1984**, *88*, 4892−4895.
(42) Rincón, L.; Gonzalez, C. A. Extended Hückel Tight-Binding Calculations of Electronic Resonances in Linear Chains of Gold Atoms and Clusters. *J. Phys. Chem. C* **2010**, *114*, 20734−20740.
(43) Zienert, A.; Schuster, J.; Gessner, T. Extended Hückel Theory for Carbon Nanotubes: Band Structure and Transport Properties. *J. Phys. Chem. A* **2013**, *117*, 3650−3654.
(44) Cerda, J.; Soria, F. Accurate and Transferable Extended Hückel-Type Tight-Binding Parameters. *Phys. Rev. B* **2000**, *61*, 7965−7971.
(45) Simonetta, M.; Gavezzotti, A. Extended Huckel and Empirical Force Field Calculations for Chemisorption on Metal Surfaces. *J. Mol. Struct.* **1984**, *107*, 75−86.
(46) Nishida, M. Theoretical Study of Luminescence Enhancement in Oxidized Si (001) Ultrathin Films. *Phys. Rev. B* **1998**, *58*, 7103.
(47) Sonnet, P.; Stauffer, L.; Saintenoy, S.; Pirri, C.; Wetzel, P.; Gewinner, G.; Minot, C. Electronic and Atomic Structure of Two-Dimensional ErSi. *Phys. Rev. B* **1997**, *56*, 15171.
(48) Sun, K.; Kohyama, M.; Tanaka, S.; Takeda, S. Theoretical Study of Atomic Oxygen on Gold Surface by Hückel Theory and DFT Calculations. *J. Phys. Chem. A* **2012**, *116*, 9568−9573.
(49) Rego, L. G. C.; Batista, V. S. Quantum Dynamics Simulations of Interfacial Electron Transfer in Sensitized TiO_2 Semiconductors. *J. Am. Chem. Soc.* **2003**, *125*, 7989−7997.
(50) Rego, L. G. C.; Abuabara, S. G.; Batista, V. S. Model Study of Coherent Quantum Dynamics of Hole States in Functionalized Semiconductor Nanostructures. *J. Chem. Phys.* **2005**, *122*, 154709.
(51) Jakubikova, E.; Snoeberger, R. C., III; Batista, V. S.; Martin, R. L.; Batista, E. R. Interfacial Electron Transfer in TiO_2 Surfaces Sensitized with Ru(II)−Polypyridine Complexes. *J. Phys. Chem. A* **2009**, *113*, 12532−12540.
(52) Da Silva, R.; Rego, L. G. C.; Freire, J. A.; Rodriguez, J.; Laria, D.; Batista, V. S. Study of Redox Species and Oxygen Vacancy Defects at TiO_2−Electrolyte Interfaces. *J. Phys. Chem. C* **2010**, *114*, 19433−19442.
(53) Prezhdo, O. V.; Rossky, P. J. Solvent Mode Participation in the Nonradiative Relaxation of the Hydrated Electron. *J. Phys. Chem.* **1996**, *100*, 17094−17102.
(54) Kundrat, M. D.; Autschbach, J. Ab Initio and Density Functional Theory Modeling of the Chiroptical Response of Glycine and Alanine in Solution Using Explicit Solvation and Molecular Dynamics. *J. Chem. Theory Comput.* **2008**, *4*, 1902−1914.
(55) Neugebauer, J.; Curutchet, C.; Muñoz-Losa, A.; Mennucci, B. A Subsystem TDDFT Approach for Solvent Screening Effects on Excitation Energy Transfer Couplings. *J. Chem. Theory Comput.* **2010**, *6*, 1843−1851.
(56) Neukirch, A. J.; Guo, Z.; Prezhdo, O. V. Time-Domain Ab Initio Study of Phonon-Induced Relaxation of Plasmon Excitations in a Silver Quantum Dot. *J. Phys. Chem. C* **2012**, *116*, 15034−15040.
(57) Kilina, S. V.; Neukirch, A. J.; Habenicht, B. F.; Kilin, D. S.; Prezhdo, O. V. Quantum Zeno Effect Rationalizes the Phonon Bottleneck in Semiconductor Quantum Dots. *Phys. Rev. Lett.* **2013**, *110*, 180404.
(58) Akimov, A. V.; Muckerman, J. T.; Prezhdo, O. V. Nonadiabatic Dynamics of Positive Charge During Photocatalytic Water Splitting on GaN(10−10) Surface: Charge Localization Governs Splitting Efficiency. *J. Am. Chem. Soc.* **2013**, *135*, 8682−8691.
(59) Andrews, D. L. A Unified Theory of Radiative and Radianionless Molecular Energy Transfer. *Chem. Phys.* **1989**, *135*, 195−201.